Electric-Field Tuning of the Surface Band Structure of Topological Insulator Sb_2Te_3 Thin Films

Tong Zhang,[1,2] Jeonghoon Ha,[1,2,3] Niv Levy,[1,2] Young Kuk,[3] and Joseph Stroscio[1,*]
[1]Center for Nanoscale Science and Technology, NIST, Gaithersburg, Maryland 20899, USA
[2]Maryland NanoCenter, University of Maryland, College Park, Maryland 20742, USA
[3]Department of Physics and Astronomy, Seoul National University, Seoul 151-747, Korea
(Received 12 April 2013; published 30 July 2013)

We measured the response of the surface state spectrum of epitaxial Sb_2Te_3 thin films to applied gate electric fields by low temperature scanning tunneling microscopy. The gate dependent shift of the Fermi level and the screening effect from bulk carriers vary as a function of film thickness. We observed a gap opening at the Dirac point for films thinner than four quintuple layers, due to the coupling of the top and bottom surfaces. Moreover, the top surface state band gap of the three quintuple layer films was found to be tunable by a back gate, indicating the possibility of observing a topological phase transition in this system. Our results are well explained by an effective model of 3D topological insulator thin films with structure inversion asymmetry, indicating that three quintuple layer Sb_2Te_3 films are topologically nontrivial and belong to the quantum spin Hall insulator class.

DOI: 10.1103/PhysRevLett.111.056803 PACS numbers: 73.20.−r, 68.37.Ef, 68.55.−a, 73.61.Ga

Topological insulators (TI) represent a novel state of quantum matter that has topologically protected edge or surface states [1,2]. Theory and experimental verification of TIs rapidly increased since the first predictions of these states of matter in two dimensions. Two-dimensional (2D) TIs are quantum spin Hall (QSH) insulators which host one-dimensional (1D) spin polarized edge states [3,4]. The concept of QSH insulators has been generalized to three-dimensional (3D) TIs, which are 3D band insulators surrounded by 2D spin helical surface states that are protected by time reversal symmetry. Recently, a family of bismuth chalcogenide materials (Bi_2Se_3, Bi_2Te_3, and Sb_2Te_3) have been confirmed to be 3D TIs with a single Dirac cone at the surface [5–11]. In sufficiently thin 3D TI films the top and bottom surface states hybridize to create an energy gap at the Dirac point. The low-lying physics is then described by two degenerate Dirac hyperbolas with a k-dependent spin configuration determined by the gap and spin-orbit coupling. Subsequently, ultrathin 3D TI films can host a wide range of intriguing topological phases [12–24] (e.g., they can be a 2D QSH system with spin polarized edge states if the system is topologically nontrivial). More interestingly, the band topology is predicted to be tunable by external electric fields, which cause structure inversion asymmetry (SIA), leading to the possibility of controlling a phase transition between topologically trivial and nontrivial phases [15–24].

In this Letter, we study the gate tunable band structure of the 3D TI Sb_2Te_3 using low- temperature scanning tunneling microscopy and spectroscopy (STM/STS) on *in situ* epitaxially grown thin films. Despite many transport measurements on gated TI devices [24–29], making a gate tunable TI film that is accessible to low temperature STM is challenging, mainly because chalcogenide TI's surfaces are environmentally sensitive and degrade easily after exposure to air. We overcome this problem by epitaxially growing TI films on prepatterned $SrTiO_3$ (111) (STO) substrates mounted on special sample holders [30]. The samples were transferred in ultrahigh vacuum into an STM right after growth, which avoided any *ex situ* processing. The Sb_2Te_3 thin films studied here are grown by codepositing Sb and Te at a substrate temperature of 200 °C. STM/STS and two-terminal transport measurements are both carried out *in situ*, in a homemade STM operating at 5 K [31].

Figure 1(a) shows the typical topography of a nominally 5 QL thick Sb_2Te_3 film. Terraces with thicknesses between 2 to 5 QL can be found on the same film. Figure 1(b) shows atomic resolution of the Te terminated (111) surface with lattice constant of 0.42 nm. The differential tunneling conductance, dI/dV, is measured by standard lock-in techniques, with a modulation frequency of ≈ 500 Hz. Typical dI/dV spectra on different layer thicknesses are shown in Fig. 1(c). The pronounced peaks [see arrows in Fig. 1(c)] are attributed to quantum well states (QWS) from bulk bands that undergo quantum confinement in a thin film geometry [32]. A closer inspection of the surface state region in Fig. 1(d) shows a hybridized gap at the sample bias $\approx V_B = 0.25$ V on 2 QL and 3 QL terraces, with a width of ≈ 160 and 80 meV, respectively, [see Fig. 3(a) for determination of gap widths]. The gap is absent for the 4 QL film and leaves a "V" shaped density of states that indicates an intact Dirac cone. Similar results were reported on Sb_2Te_3 film grown on graphitized SiC [33].

Our experimental setup allows, for the first time, for a gate voltage V_G to be applied to the Sb_2Te_3 film during STM measurements, without any *ex situ* processing and exposure of the film to atmosphere. To measure the gating characteristics, we charged the sample (a TI-STO-gate capacitor) with a current source while measuring the change of V_G. Figure 1(e) shows the total charge density

 © 2013 American Physical Society

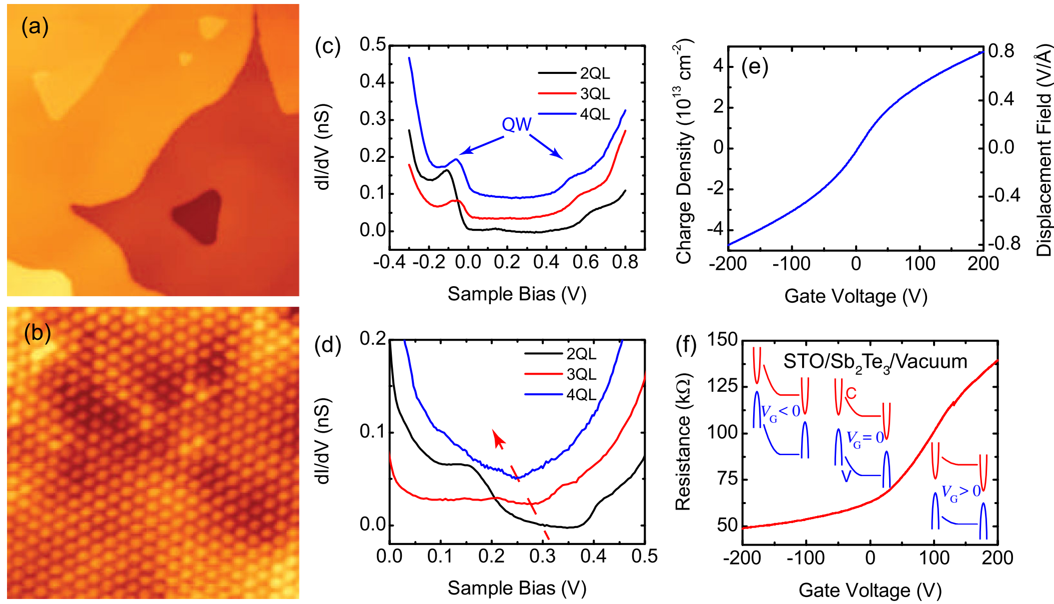

FIG. 1 (color online). Characterization of Sb_2Te_3 thin films. (a) STM topographic image, 150 nm × 150 nm, of nominally 5 QL Sb_2Te_3 film grown by molecular beam epitaxy (MBE) on $SrTiO_3(111)$. (b) Atomic resolution STM image, 10 nm × 10 nm. The STM topographic height is shown in a color scale covering a range of 5 nm for (a) and 0.14 nm for (b). Tunneling parameters are $I = 30$ pA, $V_B = 1.5$ V, for (a) and $V_B = 0.2$ V for (b). (c),(d) dI/dV spectra as a function of Sb_2Te_3 film thickness for $V_G = 0$ V, for wide (c) and narrow (d) energy ranges. The narrow energy range spectra are obtained with lower tunneling impedance. The curves are offset vertically for clarity. The red dashed line in (d) indicates the shift of the midgap position toward the Fermi level with increased thickness. (e) Total charge density and displacement field versus gate voltage for a 3 QL $Sb_2Te_3/SrTiO_3$ device obtained by charging the device. (f) 3 QL Sb_2Te_3 film two-terminal resistance versus gate voltage. (inset) Schematic of band bending through the TI film at different V_G. The diagrams shows the conduction and valence bands going through the film, and the surface state dispersions at the STO interface (left), and vacuum interface (right). At $V_G = 0$ there is initial p-type band bending which increases with negative gate voltage.

n and displacement field versus V_G by integrating the current over time. n reaches about $4.5 \times 10^{13}/\mathrm{cm}^2$ at $V_G = 200$ V, indicating a large gating ability of STO. A two-terminal film resistance measurement versus V_G is shown in Fig. 1(f), which displays a rapid increase at positive V_G, as expected for gating a p-doped semiconductor.

The gating effect is measured using the thin film QWS as a fiduciary mark in the tunneling spectra [Fig. 1(c)]. The overall gating dependence on the tunnel spectra is shown in Figs. 2(a) and 2(b) for 2 and 3 QL films by focusing on a large sample bias range (− 0.4 to 0.4 V). Increasing gate voltage is accompanied by the whole spectrum moving to lower energies, which is a clear signature of the shifting of the Fermi energy E_F due to the gate induced carrier doping. The relative shifts of E_F (with respect to $V_G = 0$) as a function of displacement field are plotted in Fig. 2(c). One can see that the gating tunability decreases fast with increasing film thickness, approximately as d^{-2} [Fig. 2(d)]. For the 2 QL film, the thinnest case, we estimate the change in surface carrier density, corresponding to the measured shift in E_F, only reaches to 1/4 of the total charge density induced by the gate. Therefore, the majority of the carriers are expected to be in the bulk of the film, which screens the electric field reaching the top surface. Subsequently, an overall Fermi level shift and band bending will coexist through the films providing a potential asymmetry between the top and bottom surfaces [34].

Now we focus on the hybridization gaps that open due to the coupling of the top and bottom surfaces, and their response to applied fields. Figures 3(a) and 3(b) show the tunneling spectra of the surface state band gaps for 2 and 3 QL terraces, respectively, as a function of V_G. The gap size is measured by the peak positions in the second derivative d^2I/dV^2, which indicate the inflection points on either side of the surface state gap [see dashed line in Fig. 3(a)]. A noticeable feature is that the surface states gap is rather constant at 2 QL, but varies considerably with V_G for 3 QL. Differences in the response of the gap to fields, as observed between the 2 and 3 QL films, can occur due to changes in the topology of the system. Such changes can arise with variations as small as 1 QL in film thickness [18,19]. The gap for the 3 QL film shows a linear dependence on the displacement field [Fig. 3(d)]. This is reminiscent of bilayer graphene where the asymmetric potential controls the gap at the Dirac point [35,36]. The difference here is that in a TI thin film, the interlayer and spin-orbit coupling play important roles.

To understand how an electric field affects the surface band structure, we refer to an effective Hamiltonian model that describes thin 3D TI films in Refs. [17,18], which gives rise to four surface state energy bands,

$$E_{1\pm} = E_0 - Dk^2 \pm \sqrt{\left(\frac{\Delta}{2} - Bk^2\right)^2 + (|\gamma U| + \hbar v_F k)^2}, \quad (1)$$

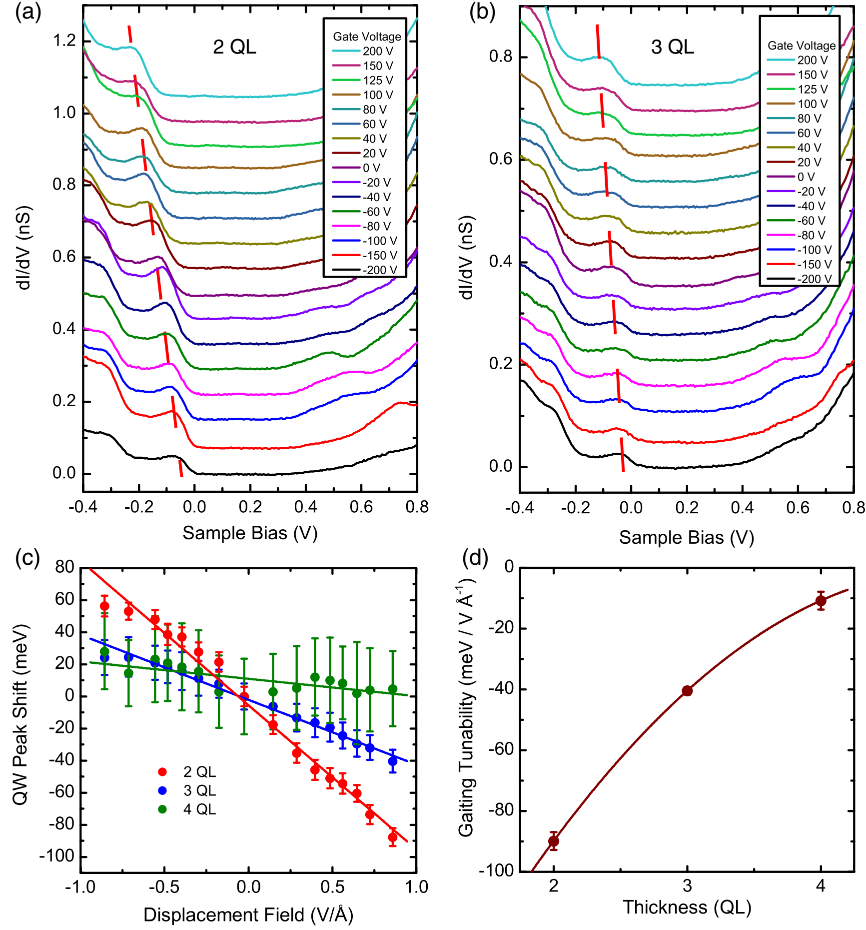

FIG. 2 (color online). *In situ* measurement of electric field gating of MBE grown Sb_2Te_3 thin films. dI/dV versus V_B spectra as a function of the indicated back gate voltage for a (a) 2 QL thick film, and (b) 3 QL thick film. A shift of the QW peaks to higher energy is seen with increased gate potential, as indicated by the dashed lines. (c) The relative shift of the QW peak positions versus displacement field for 2–4 QL films. Error bars are 1 standard deviation uncertainties in determining the QW peak positions. The solid lines are linear fits to the data points. (d) The gating tunability versus film thickness obtained from the slopes of the linear fits in (c). The error bars are 1 standard deviation uncertainties from the linear fits. The solid line is a polynomial fit to the data points.

$$E_{2\pm} = E_0 - Dk^2 \pm \sqrt{\left(\frac{\Delta}{2} - Bk^2\right)^2 + (|\gamma U| - \hbar v_F k)^2}, \quad (2)$$

where the $+(-)$ sign stands for the conduction (valence) band, and the 1 (2) stands for the inner (outer) branches of the bands. The bands are characterized by the parameters E_0, D, B, Δ, v_F, and γ, which are material and thickness dependent. The potential difference between the top and bottom surfaces, U, enters the Hamiltonian in the form of an effective potential γU leading to SIA. Without the SIA term ($\gamma U = 0$) the surface states consist of spin degenerate conduction and valence bands separated by a hybridization gap Δ [Fig. 3(e)]. The presence of the potential U leads to a Rashba-like splitting of these bands [Figs. 3(f)]. Moreover, from Eqs. (1) and (2), the actual gap size also varies with γU [see Figs. 3(e)–3(h)]. This is directly related to our observations of the 3 QL Sb_2Te_3 gap varying with applied gate voltage [Figs. 3(b) and 3(d)], which is examined below.

As discussed in Refs. [17,18], the sign of Δ/B and the value of the SIA term determine if the system is topologically trivial or nontrivial. If $B^2 > D^2$ and Δ and B have the same sign, ($\Delta/B > 0$), the system is in the quantum spin hall state. Increasing the SIA term γU reduces the energy gap [Fig. 3(f)] and eventually closes it at the critical value $\gamma U_C = \hbar v_F \sqrt{\Delta/2B}$ [Fig. 3(g)] and then reopens it, leading to a topological phase transition as a function of applied electric field [17,19]. If Δ and B have opposite signs, the system remains gapped with applied electric field. Figure 3(h) compares these two cases. We note that γU contributes to Eq. (1) and (2) through its absolute value, so the gap variation should be symmetric with respect to the gate voltage. However, in Fig. 3(d) the gap displays a monotonic dependence on displacement field within the range investigated. We expect this is due to an initial band bending which exists even at $V_G = 0$ [see Fig. 1(f) inset] and is common for heterojunctions.

We can estimate the initial bending direction from the thickness dependence of the position of the Dirac point (or midgap energy position). As shown by the dashed line in Fig. 1(d), the middle of the gap moves closer to E_F with

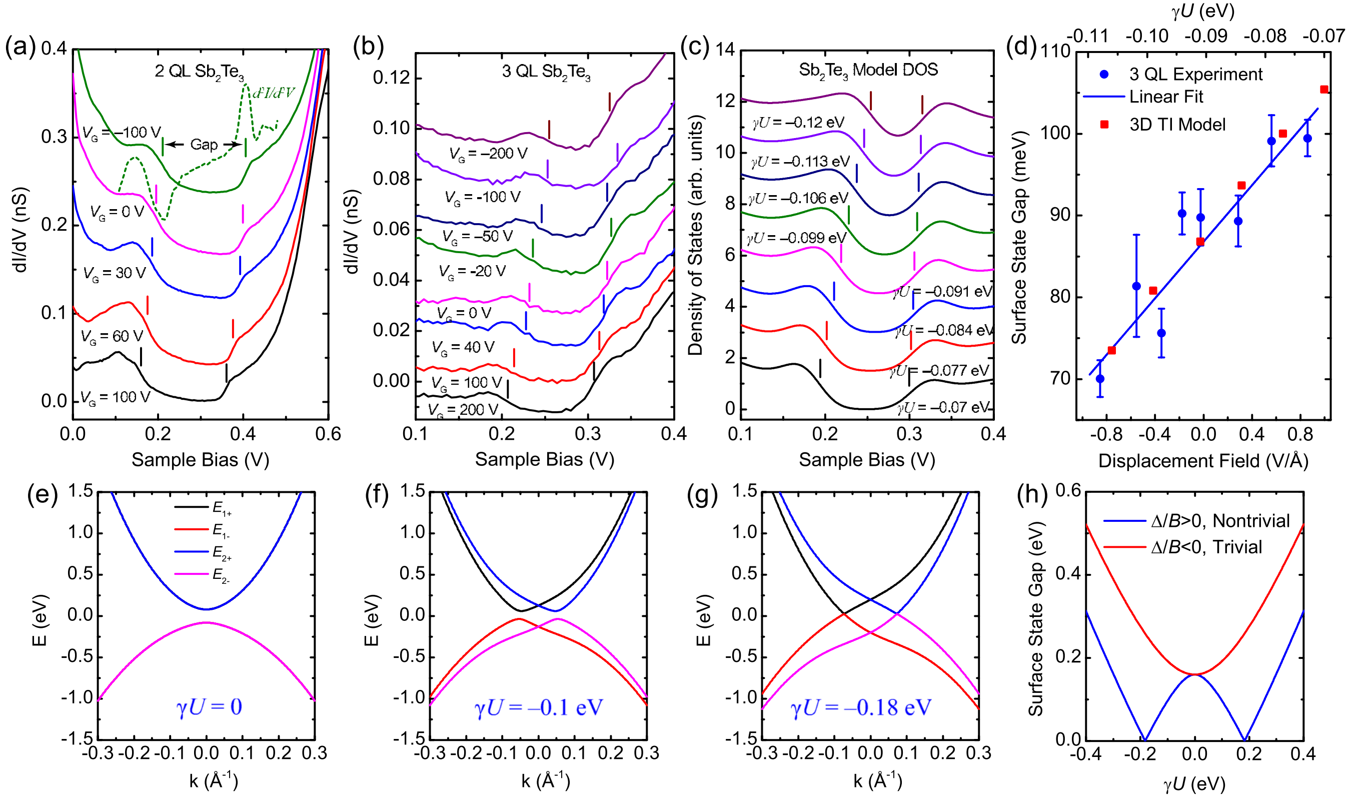

FIG. 3 (color online). Electric field effect of surface state band gaps in MBE grown Sb_2Te_3 thin films. dI/dV versus V_B spectra of the surface state gap as a function of the indicated back gate voltage for (a) 2 QL Sb_2Te_3 film, and (b) 3 QL Sb_2Te_3 film. The curves are offset for clarity. (c) Calculated surface state DOS using the dispersions in Eqs. (1) and (2) as a function of applied potential. See text for model parameters. (d) Measured surface state band gap from the spectra in (b) of 3 QL Sb_2Te_3 thin films as a function of displacement field (blue round symbols), and surface state band gap from the model DOS calculation in (c) versus γU (red square symbols). The band gaps are determined from the peak minimum and maximum in the second derivative spectra [see green dashed curve in (a) and tic marks in (a)–(c)] for both the experiment and model calculation. The error bars are 1 standard deviation uncertainty determined from peak fitting. The solid line is a linear fit to the data with a slope of 17.3 ± 2.5 meV/V Å^{-1}. The error is 1 standard deviation uncertainty determined from the linear fit. (e)–(g) Energy versus momentum dispersion calculated using Eqs. (1) and (2) showing the variation of the band gap as a function of increasing structure inversion asymmetry potential. See text for model parameters. At the potential $\gamma U = 0.18$ eV $= \gamma U_C$ the gap closes, indicating a topological phase transition. (h) Surface state band gaps calculated from the 3D TI model using Eqs. (1) and (2) with $\Delta = 0.16$ eV, $D = -5$ eV Å^2, $v_F = 2.5$ eV Å, and $\Delta/B > 0$ (blue; $B = 15$ eV Å^2), and $\Delta/B < 0$ (red; $B = -15$ eV Å^2).

increasing thickness from 2 to 4 QL, which implies the top surface of the film is less doped at increased thicknesses. The increased doping for thinner films is probably due to an increased number of defects at the TI/STO interface. These defects are very effective acceptors [32]. The higher hole doping at the interface gives an initial upward band bending through the film at $V_G = 0$ [Fig. 1(f) inset], and will affect the surface band gap as if a gate field were applied [34]. Applying a negative gate potential leads to hole accumulation and further enhances the band bending intensity, and, hence, the potential asymmetry. Therefore, if the system is nontrivial, applying a negative gate potential leads to a decreased gap according to the above analysis [Fig. 3(h)]. This is what is observed in Fig 3(b) for 3 QL. We model the spectra in Fig. 3(b) for 3 QL by calculating the density of states (DOS) from Eqs. (1) and (2), taking $v_F = 2.5$ eV Å, $B = 15$ eV Å^2, and $D = -5$ eV Å^2 from fits to photoemission spectroscopy and density functional calculation results in Ref. [37]. The model DOS curves are convoluted with a Gaussian (with standard deviation $\sigma = 20$ meV) to account for instrumental broadening and are shown in Fig. 3(c). The fitting parameters used are $\Delta = 0.16$ eV, with E_0 varying from 0.24 to 0.27 eV, and γU varying from 0.07 to 0.12 eV, as V_G changes from 200 to -200 V. The variation of γU is within the range of total potential asymmetry we achieved by gating (≈ 50 meV). The simulated DOS in Fig. 3(c) are in good agreement with experiment [Fig. 3(b)]. From the model calculation in Figs. 3(c) and 3(d), we observe the gap decreasing with increased potential asymmetry in agreement with the experimental observations.

From the model parameters, Δ and B have the same sign, $\Delta/B > 0$, which indicates a topologically nontrivial QSH phase. We determine that the 3 QL Sb_2Te_3 system is topologically nontrivial by noting that the band gap decreases with negative applied gate voltage. For the

observed initial p-type doping [see Figs. 1(d) and 1(f)], such a decrease can only occur if Δ and B have the same sign [see Fig. 3(h)]. The topological character of the system is typically characterized by the Z_2 invariant, where $Z_2 = 1$ signifies the topological nontrivial phase [1,2]. The deduced phase diagram from our results in terms of the Z_2 invariant would be as follows: at $V_G = 0$ V, 3 QL Sb_2Te_3 is in a topologically nontrivial phase with $Z_2 = 1$ and should undergo a phase transition to $Z_2 = 0$ with increasing gate field. This conclusion is similar to what has been predicted for 4 QL Sb_2Te_3 thin films [19]. Gapless edge states are supposed to exist in this regime [13,17,19] and searching for these edge states will be an interesting subject for further studies. We expect that the topological phase transition should also be observable in future studies with more insulating material to obtain higher electric fields.

We thank Mark Stiles, Paul Haney, Minsung Kim, and Jisoon Ihm for useful discussions. We thank Steve Blankenship and Alan Band for technical assistance. N.L., T.Z., and J.H. acknowledge support under the Cooperative Research Agreement between the University of Maryland and the National Institute of Standards and Technology Center for Nanoscale Science and Technology, Grant No. 70NANB10H193, through the University of Maryland. J.H. and Y.K. are partly supported by Korea Research Foundation through Grant No. KRF-2010-00349.

*Author to whom correspondence should be addressed.
joseph.stroscio@nist.gov

[1] M.Z. Hasan and C.L. Kane, Rev. Mod. Phys. **82**, 3045 (2010).
[2] X.-L. Qi and S.-C. Zhang, Rev. Mod. Phys. **83**, 1057 (2011).
[3] C.L. Kane and E.J. Mele, Phys. Rev. Lett. **95**, 226801 (2005).
[4] B.A. Bernevig and S.-C. Zhang, Phys. Rev. Lett. **96**, 106802 (2006).
[5] H. Zhang, C.-X. Liu, X.-L. Qi, X. Dai, Z. Fang, and S.-C. Zhang, Nat. Phys. **5**, 438 (2009).
[6] Y. Xia, D. Qian, D. Hsieh, L. Wray, A. Pal, H. Lin, A. Bansil, D. Grauer, Y.S. Hor, R.J. Cava, and M.Z. Hasan, Nat. Phys. **5**, 398 (2009).
[7] D. Hsieh, Y. Xia, D. Qian, L. Wray, J.H. Dil, F. Meier, J. Osterwalder, L. Patthey, J.G. Checkelsky, N.P. Ong, A.V. Fedorov, H. Lin, A. Bansil, D. Grauer, Y.S. Hor, R.J. Cava, and M.Z. Hasan, Nature (London) **460**, 1101 (2009).
[8] Y.L. Chen, J.G. Analytis, J.-H. Chu, Z.K. Liu, S.-K. Mo, X.L. Qi, H.J. Zhang, D.H. Lu, X. Dai, Z. Fang, S.C. Zhang, I.R. Fisher, Z. Hussain, and Z.-X. Shen, Science **325**, 178 (2009).
[9] P. Roushan, J. Seo, C.V. Parker, Y.S. Hor, D. Hsieh, D. Qian, A. Richardella, M.Z. Hasan, R.J. Cava, and A. Yazdani, Nature (London) **460**, 1106 (2009).
[10] T. Zhang, P. Cheng, X. Chen, J.-F. Jia, X. Ma, K. He, L. Wang, H. Zhang, X. Dai, Z. Fang, X. Xie, and Q.-K. Xue, Phys. Rev. Lett. **103**, 266803 (2009).
[11] Z. Alpichshev, J.G. Analytis, J.-H. Chu, I.R. Fisher, Y.L. Chen, Z.X. Shen, A. Fang, and A. Kapitulnik, Phys. Rev. Lett. **104**, 016401 (2010).
[12] B. Zhou, H.-Z. Lu, R.-L. Chu, S.-Q. Shen, and Q. Niu, Phys. Rev. Lett. **101**, 246807 (2008).
[13] J. Linder, T. Yokoyama, and A. Sudbø, Phys. Rev. B **80**, 205401 (2009).
[14] C.-X. Liu, H.J. Zhang, B. Yan, X.-L. Qi, T. Frauenheim, X. Dai, Z. Fang, and S.-C. Zhang, Phys. Rev. B **81**, 041307 (2010).
[15] J. Li and K. Chang, Appl. Phys. Lett. **95**, 222110 (2009).
[16] H.-Z. Lu, W.-Y. Shan, W. Yao, Q. Niu, and S.-Q. Shen, Phys. Rev. B **81**, 115407 (2010).
[17] W.-Y. Shan, H.-Z. Lu, and S.-Q. Shen, New J. Phys. **12**, 043048 (2010).
[18] H. Li, L. Sheng, D.N. Sheng, and D.Y. Xing, Phys. Rev. B **82**, 165104 (2010).
[19] M. Kim, C.H. Kim, H.-S. Kim, and J. Ihm, Proc. Natl. Acad. Sci. U.S.A. **109**, 671 (2012).
[20] H. Li, L. Sheng, and D.Y. Xing, Phys. Rev. B **85**, 045118 (2012).
[21] G. Liu, G. Zhou, and Y.-H. Chen, Appl. Phys. Lett. **101**, 223109 (2012).
[22] Y. Sakamoto, T. Hirahara, H. Miyazaki, S.I. Kimura, and S. Hasegawa, Phys. Rev. B **81**, 165432 (2010).
[23] Y. Zhang, K. He, C.-Z. Chang, C.-L. Song, L.-L. Wang, X. Chen, J.-F. Jia, Z. Fang, X. Dai, W.-Y. Shan, S.-Q. Shen, Q. Niu, X.-L. Qi, S.-C. Zhang, X.-C. Ma, and Q.-K. Xue, Nat. Phys. **6**, 584 (2010).
[24] A.A. Taskin, S. Sasaki, K. Segawa, and Y. Ando, Phys. Rev. Lett. **109**, 066803 (2012).
[25] J. Chen, H.J. Qin, F. Yang, J. Liu, T. Guan, F.M. Qu, G.H. Zhang, J.R. Shi, X.C. Xie, C.L. Yang, K.H. Wu, Y.Q. Li, and L. Lu, Phys. Rev. Lett. **105**, 176602 (2010).
[26] J.G. Checkelsky, Y.S. Hor, R.J. Cava, and N.P. Ong, Phys. Rev. Lett. **106**, 196801 (2011).
[27] H. Steinberg, D.R. Gardner, Y.S. Lee, and P. Jarillo-Herrero, Nano Lett. **10**, 5032 (2010).
[28] D. Kong, Y. Chen, J.J. Cha, Q. Zhang, J.G. Analytis, K. Lai, Z. Liu, S.S. Hong, K.J. Koski, S.-K. Mo, Z. Hussain, I.R. Fisher, Z.-X. Shen, and Y. Cui, Nat. Nanotechnol. **6**, 705 (2011).
[29] D. Kim, S. Cho, N.P. Butch, P. Syers, K. Kirshenbaum, S. Adam, J. Paglione, and M.S. Fuhrer, Nat. Phys. **8**, 459 (2012).
[30] T. Zhang, N. Levy, J. Ha, Y. Kuk, and J.A. Stroscio, Phys. Rev. B **87**, 115410 (2013).
[31] Y.J. Song, A.F. Otte, V. Shvarts, Z. Zhao, Y. Kuk, S.R. Blankenship, A. Band, F.M. Hess, and J.A. Stroscio, Rev. Sci. Instrum. **81**, 121101 (2010).
[32] Y. Jiang, Y.Y. Sun, M. Chen, Y. Wang, Z. Li, C. Song, K. He, L. Wang, X. Chen, Q.-K. Xue, X. Ma, and S.B. Zhang, Phys. Rev. Lett. **108**, 066809 (2012).
[33] Y. Jiang, Y. Wang, M. Chen, Z. Li, C. Song, K. He, L. Wang, X. Chen, X. Ma, and Q.-K. Xue, Phys. Rev. Lett. **108**, 016401 (2012).
[34] D. Galanakis and T.D. Stanescu, Phys. Rev. B **86**, 195311 (2012).
[35] E. McCann, Phys. Rev. B **74**, 161403 (2006).
[36] T. Ohta, A. Bostwick, T. Seyller, K. Horn, and E. Rotenberg, Science **313**, 951 (2006).
[37] C. Pauly, G. Bihlmayer, M. Liebmann, M. Grob, A. Georgi, D. Subramaniam, M.R. Scholz, J. Sánchez-Barriga, A. Varykhalov, S. Blügel, O. Rader, and M. Morgenstern, Phys. Rev. B **86**, 235106 (2012).